

Origin of the mass splitting of azimuthal anisotropies in a multi-phase transport model

Hanlin Li,^{1,2} Liang He,² Zi-Wei Lin,³ Denes Molnar,² Fuqiang Wang,² and Wei Xie²

¹*College of Science, Wuhan University of Science and Technology, Wuhan, Hubei 430065, China*

²*Department of Physics and Astronomy, Purdue University, West Lafayette, IN 47907, USA*

³*Department of Physics, East Carolina University, Greenville, NC 27858, USA*

(Dated: January 27, 2023)

The mass splitting of azimuthal anisotropy (v_n) at low transverse momentum (p_\perp) is considered as a hallmark of hydrodynamic collective flow. We investigate a multi-phase transport (AMPT) model where the v_n is mainly generated by the escape mechanism, not of the hydrodynamic flow nature, and where the mass splitting is also observed. This paper provides extensive details to our published work on Au+Au and d+Au collisions at the Relativistic Heavy Ion Collider (arXiv:1601.05390); it also includes new results on p+Pb collisions at the Large Hadron Collider. We demonstrate that the mass splitting of v_n in AMPT partly arises from kinematics in the quark coalescence hadronization process but more dominantly from hadronic rescatterings, even though the contribution from the latter to the overall charged hadron v_n is small. It is also found that hadronic decays reduce the degree of mass splitting. These findings are qualitatively the same as those from hybrid models that combine hydrodynamics with a hadron cascade. It is further shown that there is no qualitative difference between heavy ion collisions and small-system collisions or between elliptic (v_2) and triangular (v_3) anisotropies. Our studies indicate that the mass splitting of low- p_\perp v_n is not a unique signature of hydrodynamic collective flow, but can be a quantitative interplay of several physics effects. The mass splitting thus cannot distinguish whether the anisotropic flow is generated mainly from hydrodynamics or the anisotropic parton escape.

PACS numbers: 25.75.-q, 25.75.Ld

I. INTRODUCTION

Relativistic heavy ion collisions aim to create the quark-gluon plasma (QGP) and study quantum chromodynamics (QCD) at the extreme conditions of high temperature and energy density [1–5]. The system created in these collisions is described well by hydrodynamics where the high pressure buildup drives the system to expand at relativistic speed [6, 7]. Fits of the experimental data with hydrodynamics inspired models suggest that particles are locally thermalized and possess a common radial flow velocity [8]. Of particular interests are non-central collisions where the overlap volume of the colliding nuclei is anisotropic in the transverse plane (perpendicular to beam). The pressure gradient would generate an anisotropic expansion and the final-state elliptic flow [9]. Large elliptic anisotropies in the momentum space (v_2) have been measured, as large as hydrodynamic calculations predict [1–7]. This suggests that the collision system is strongly interacting and nearly thermalized (sQGP) [10].

Due to fluctuations in the initial-state collision geometry, there is an elliptic harmonic anisotropy in the configuration space (ϵ_2) even in head-on central collisions (impact parameter $b = 0$ fm) [11]. In fact, due to fluctuations, there are finite configuration space harmonics of all orders [12]. This will result in final-state momentum anisotropies of all orders (v_n , where $n = 1, 2, 3, 4, \dots$).

A hallmark of the hydrodynamic description of relativistic heavy ion collisions is the mass splitting of v_2 at a given, low transverse momentum (p_\perp) [6]. It suggests a common radial velocity field, whose azimuthal

modulation gives rise to momentum-space azimuthal anisotropies, and whose effect on hadron p_\perp via the Cooper-Frye hadronization mechanism [13] (commonly exploited in hydrodynamic calculations) gives rise to the mass splitting. Results from hybrid models, where hydrodynamics is followed by a hadron cascade, have shown that the v_2 mass splitting is small just after hadronization when resonance decays are included and that the mass splitting is strongly enhanced by hadronic scatterings [14–16]. It has also been shown that the magnitude of the mass splitting from the hydrodynamical stage alone depends strongly on the kinetic freeze-out temperature [14].

It is generally perceived that large v_n can only be generated in large-system heavy ion collisions, and hydrodynamics is a highly plausible scenario for how the collision system evolves. Recent particle correlation data, however, hint at similar v_n and mass splitting effect in small systems of high multiplicity $p+p$ [17] and $p+Pb$ [18–20] collisions at the Large Hadron Collider (LHC) and $d+Au$ [21, 22] collisions at the Relativistic Heavy Ion Collider (RHIC). Hydrodynamics has been applied to these small systems and seems to successfully describe the experimental data, including the mass splitting [23, 24]. This could suggest that these small-system collisions create a sQGP as well, in contrast to naive expectations.

On the other hand, parton transport models, such as a multi-phase transport (AMPT) [25, 26], have been widely used to describe experimental data. The string melting version of AMPT [26, 27] reasonably reproduces particle yields, p_\perp spectra, and v_2 of low- p_\perp pions and kaons in central and mid-central Au+Au collisions at 200A GeV and Pb+Pb collisions at 2760A GeV (see Figs.1-3 of

Ref. [28]). The small system data can also be satisfactorily described by AMPT [29]. The successful description by AMPT of experimental data, especially the heavy ion data, did not come as surprises, because it has been perceived that transport models have approached hydrodynamic limit at high energy densities and/or large parton interaction cross-sections.

However, a recent study by some of us using AMPT shows that the azimuthal anisotropy is mainly generated by the anisotropic parton escape [30, 31]; hydrodynamics may play only a minor role. This escape mechanism would naturally and simultaneously explain the measured azimuthal anisotropies in both heavy ion and small system collisions. On the other hand, the escape mechanism does not generate radial flow, but mass splitting is also present in v_n from AMPT. This suggests that hydrodynamic radial flow may not be the only mechanism that can generate the mass splitting of v_n . We argue that the origins of the mass splitting of v_2 in AMPT are due to kinematics in the coalescence hadronization and hadronic rescatterings [32]. Our main results, using AMPT simulations of Au+Au and d +Au collisions at the top RHIC energy, have already been published [32]. This paper provides more details to the published work as well as additional results from AMPT simulations of p +Pb collisions at the LHC.

II. MODEL AND ANALYSIS

We employ the string melting version of AMPT [26, 27] in our study. The model consists of a fluctuating initial condition, parton elastic scatterings, quark coalescence for hadronization, and hadronic interactions. The initial energy and particle productions are being described by the HIJING model. However, the string melting AMPT model converts these initial hadrons to their valence quarks and antiquarks, based on the assumption that the high energy density in the overlap region of high energy heavy ion collisions requires us to use parton degrees of freedom to describe the dense matter [27].

Parton scatterings are treated with Zhang's Parton Cascade (ZPC) [33]. We use Debye-screened differential cross-section $d\sigma/dt \propto \alpha_s^2/(t - \mu_D^2)^2$ [26] in AMPT, with the strong coupling constant $\alpha_s = 0.33$ and Debye screening mass $\mu_D = 2.265/\text{fm}$. The total parton scattering cross section is then $\sigma = 3 \text{ mb}$ for all AMPT calculations in this study. After partons stop interacting, a simple quark coalescence model is applied to convert partons into hadrons [26]. Subsequent interactions of these formed hadrons are modeled by a hadron cascade [26]. We terminate the hadronic interactions at a cutoff time (t_{max}), when the observables of interest are stable; a cutoff time of $t_{\text{max}} = 30 \text{ fm}/c$ is used here.

Hadronization in the string melting version of AMPT is modeled with a simple quark coalescence, where two nearest partons (one quark and one antiquark) are combined into a meson and three nearest quarks (or an-

tiquarks) are combined into a baryon (or antibaryon). In addition, when the flavor composition of the coalescing quark and antiquark allows the formation of either a pseudo-scalar or a vector meson, the meson species whose mass is closer to the invariant mass of the coalescing parton pair will be formed. The same criterion is also applied to the formation of an octet or a decuplet baryon with the same flavor composition. Thus in these situations the hadron species that has a larger mass will be typically formed when the coalescing partons have a larger invariant mass.

The hadron cascade in the AMPT model includes explicit particles such as π , ρ , ω , η , K , K^* , ϕ mesons, N , Δ , $N^*(1440)$, $N^*(1535)$, Λ , Σ , Ξ , Ω , and deuteron and the corresponding anti-particles [34]. Hadronic interactions include meson-meson, meson-baryon, and baryon-baryon elastic and inelastic scatterings. For example, meson-baryon scatterings includes pion-nucleon, ρ -nucleon, and kaon-nucleon elastic and inelastic processes, among many reaction channels. More details can be found in the main AMPT paper [26].

We simulate three collision systems: Au+Au collisions at RHIC with $b = 6.6\text{-}8.1 \text{ fm}$ (corresponding to approximately 20%-30% centrality [8]) at the nucleon-nucleon center-of-mass energy $\sqrt{s_{\text{NN}}} = 200 \text{ GeV}$, d +Au collisions at RHIC with $b = 0 \text{ fm}$ at $\sqrt{s_{\text{NN}}} = 200 \text{ GeV}$, and p +Pb collisions at LHC with $b = 0 \text{ fm}$ at $\sqrt{s_{\text{NN}}} = 5 \text{ TeV}$. The initial geometric anisotropy of the transverse overlap region of a heavy-ion collision is often described by eccentricity of the n th harmonic order [12]:

$$\epsilon_n = \sqrt{\langle r_{\perp}^2 \cos n\phi_r \rangle^2 + \langle r_{\perp}^2 \sin n\phi_r \rangle^2} / \langle r_{\perp}^2 \rangle. \quad (1)$$

Here r_{\perp} and ϕ_r are the polar coordinate of each initial parton (after its formation time) in the transverse plane, and $\langle \dots \rangle$ denotes the per-event average.

We compute the n^{th} harmonic plane (short-axis direction of the corresponding harmonic component) of each event from its initial configuration of all partons [35] by

$$\psi_n^{(r)} = \frac{1}{n} [\text{atan2}(\langle r_{\perp}^2 \sin n\phi_r \rangle, \langle r_{\perp}^2 \cos n\phi_r \rangle) + \pi]. \quad (2)$$

We analyze [32] the momentum-space azimuthal anisotropy of partons in the final state of parton cascade before hadronization, of hadrons right after hadronization before hadronic rescatterings take place, and of freeze-out hadrons in the final state. The momentum anisotropies are characterized by Fourier coefficients [36]

$$v_n^{\text{obs}} = \langle \cos n(\phi - \psi_n^{(r)}) \rangle, \quad (3)$$

where ϕ is the azimuthal angle of the particle (parton or hadron) momentum. The resolution (accuracy) of $\psi_n^{(r)}$ is practically 100% due to the large initial parton multiplicity [37]. All results shown in this paper are for particles (partons or hadrons) within the pseudorapidity (η) window of $|\eta| < 1$.

III. PARTONIC ANISOTROPY

AMPT has only quarks but no gluons. The gluon degree of freedom can be considered as absorbed in the quark's. Figure 1 shows the v_2 and v_3 of the u and d light (anti-)quarks and the s strange (anti-)quarks in three systems: Au+Au and d +Au collisions at 200 GeV, and p +Pb collisions at 5 TeV. The quark and antiquark anisotropies are found to be the same, so they are combined. There is practically no difference between the u and d (anti-)quark v_n 's, so they are also combined in Fig. 1. The v_n magnitudes are similar among the three systems, except v_3 in d +Au which is significantly lower than the other two systems. In general small systems should generate lower v_n than large systems, and this is the case for v_3 between d +Au and Au+Au collisions. The v_2 in d +Au is not much smaller than that in Au+Au, possibly because the lower energy density in d +Au is compensated by the larger elliptical eccentricity (ϵ_2). The v_n in p +Pb are not much smaller than those in Au+Au, and this may be because the smaller system size is compensated by the larger collision energy.

At low p_\perp the light quark v_2 is larger than the s quark's. This is qualitatively consistent with the hydrodynamic picture where particles move with a common collective flow velocity. Because particles have the same v_n at the same speed, $v_n(p_\perp)$ as a function of p_\perp are split according to particle masses. This mass splitting between light and strange quarks is observed in both v_2 and v_3 and in all three systems. However, our previous studies [30, 31] have shown that v_2 comes largely from the anisotropic escape mechanism. The question is then whether or not the observed mass splitting is entirely due to the minor contributions from hydrodynamics. To address this question we also carry out a test calculation with no collective anisotropic flow by randomizing the outgoing parton azimuthal directions after each parton-parton scattering as in Ref. [30]. The results are shown by the dashed curves in Fig. 1; differences between u, d and s quark v_n 's are still present. Since the parton azimuthal angles are now randomized, the final-state parton anisotropy is entirely due to the anisotropic escape mechanism [30]. The fact that the mass splitting is similar between the normal and ϕ -randomized AMPT suggests that it may be caused by kinematic difference in the scattering processes due to their mass difference rather than collective flow. This will be discussed next. At high p_\perp their v_n 's approach to each other as expected because the mass difference becomes unimportant and the scattering cross-sections are set to be the same regardless of quark flavors.

IV. MASS SPLITTING FROM THE QUARK COALESCENCE HADRONIZATION

Since hadrons such as pions and protons come all from the light quarks, the difference between their

anisotropies must come from the hadronization process and/or hadronic rescatterings. We study the effect of the former by examining v_2 of hadrons right after hadronization before rescatterings take place. Figure 2 shows the primordial $\pi, K, p(\bar{p}), \Lambda(\bar{\Lambda}), \Xi(\bar{\Xi})$ v_2 and v_3 as a function of p_\perp in the three systems we studied. Note that primordial hadrons are hadrons right after hadronization but before resonance decays and hadronic scatterings. In Au+Au collisions the particle v_n exhibit the familiar mass-ordering at low p_\perp —the v_n 's of pions are larger than those of kaons which are in turn larger than those of (anti-)protons and strange baryons. The mass splittings in the small systems of d +Au and p +Pb are not necessarily the same ordering as in the Au+Au system. In any case, the difference between the different particle species, especially between π and proton, must come from the hadronization process in AMPT. In this section we study how this mass splitting comes about. We will concentrate on v_2 but the discussions can be extended to v_3 .

AMPT forms hadrons via quark coalescence. The difference in the pion and proton v_2 comes from differences in the number of constituent quarks they are made of and in the kinematics of those (anti-)quarks. At high p_\perp the hadron v_2 has been measured to exhibit the number of constituent quark scaling:

$$v_2^B/3 \approx v_2^M/2, \quad (4)$$

where the superscripts 'B' stands for baryons and 'M' for mesons. This comes naturally from quark coalescence, where two or three relatively high p_\perp quarks are more or less collimated and coalesce into a meson or baryon. The meson and baryon take on twice and three times the quark v_2 (which are saturated at high p_\perp as in Fig. 1), respectively. Apparently, this quark collimation picture cannot be extended to low p_\perp ; if it could, then, because the quark v_2 is approximately linear at low p_\perp (see Fig. 1), the meson and baryon $v_2(p_\perp)$ as a function of p_\perp would coincide with each other (the two or three constituent quark p_\perp 's add to the hadron p_\perp and the quark v_2 's also add to the hadron v_2) and there would be no mass splitting. The mass splitting of v_2 at low p_\perp , therefore must come from the kinematics in the coalescence process [38] such as finite opening angles. To quantitatively understand this, we show in Fig. 3 upper panels the p_\perp distributions for partons coalescing into pions and protons of $p_\perp = 1$ GeV/ c , as an example, and their constituent quark opening angle distributions in the lower panels. We have also depicted in the plots another meson, the ρ , which has the same constituent quark content as the π but a larger mass. Shown in Fig. 3 are both the normal and ϕ -randomized AMPT data. Figure 3 lower panel shows the azimuthal angle of the constituent quark from that of the coalesced hadron, $\Delta\phi = \phi_q - \phi_h$. Because of the finite angles, the average p_\perp of constituent quarks is larger than a half (one third) of the pion (proton) p_\perp . While the actual kinematics are complex, one may easily verify that a pair (or triplet) of partons of the

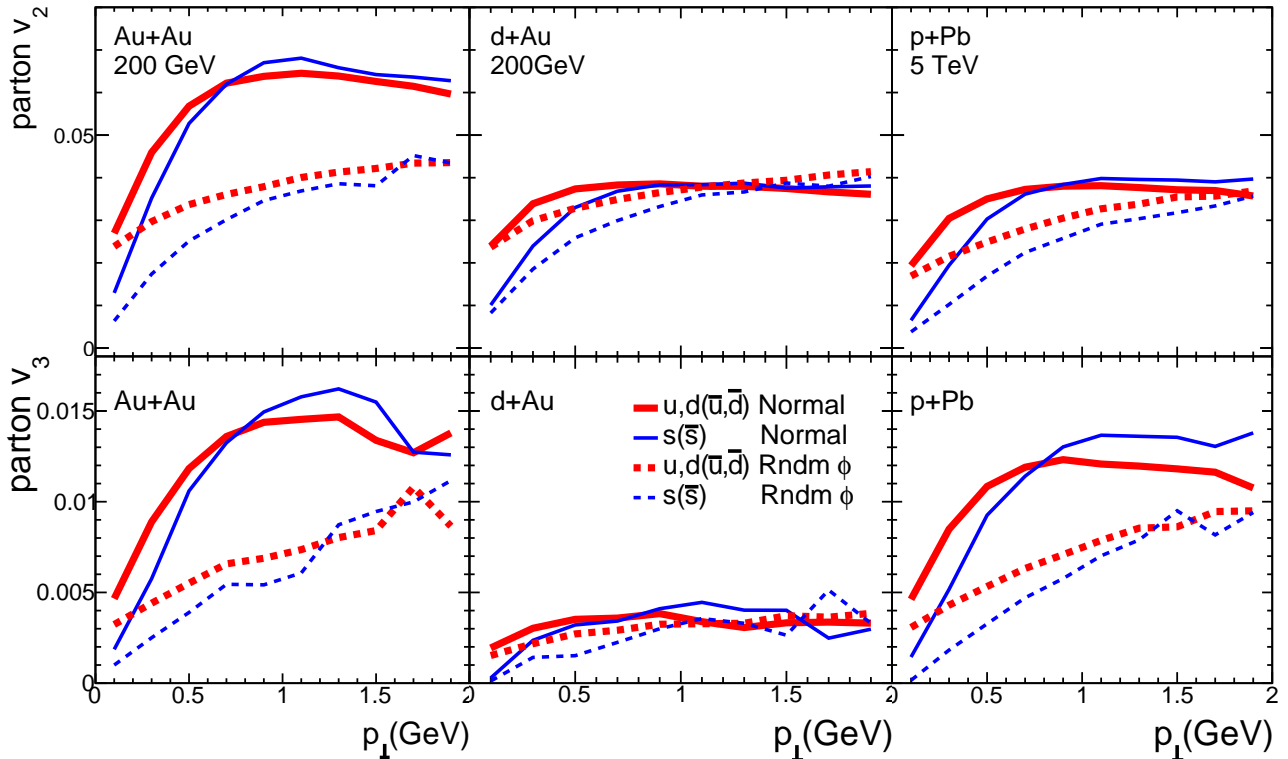


FIG. 1: (Color online) *Parton* v_n . Parton v_n as a function of p_\perp for light (u and d) and strange (s) (anti-)quarks in the final state before hadronization AMPT (with string melting). Three systems are shown: $b = 6.6\text{--}8.1$ fm Au+Au collisions at $\sqrt{s_{NN}} = 200$ GeV (left column), $b = 0$ fm d+Au collisions at 200 GeV (middle column), and $b = 0$ fm p+Pb at 5 TeV (right column); v_2 results are shown in upper panels and v_3 in lower panels. Both normal (solid curves) and ϕ -randomized (dashed curves) AMPT results are shown.

average p_\perp^q with the average opening angle (as in Fig. 3) gives the composite hadron p_\perp^h roughly as

$$p_\perp^h \approx n_q p_\perp^q \cos(\Delta\phi), \quad (5)$$

where the superscripts ‘h’ and ‘q’ stand for hadrons and constituent quarks, respectively, and n_q is the number of constituent quarks for the given hadron type.

Similarly, because of the finite opening angle the hadron v_2 is not simply twice (or three times) the average quark v_2 at the corresponding average quark p_\perp . This is shown in Fig. 4 where the quark v_2 is plotted at the p_\perp of the hadron it coalesces into, together with the hadron v_2 from Fig. 2. Note that the quark v_2 in Fig. 1 includes all quarks (i.e. from all hadrons) while that in Fig. 4 is categorized by the final-state hadrons. As seen from Fig. 4, the pions (proton) v_2 shown in symbols are smaller than twice (three times) the quarks shown in the curves. Note the shapes of the curves are different because they are plotted at the hadron p_\perp and because p_\perp samplings of quarks into pions and protons are different (c.f. Fig. 3). One may get a semiquantitative understanding of the hadron $v_2(p_\perp)$ curve by, again, using the average quark kinematics. The hadron azimuthal distri-

bution is

$$\prod_{q=1}^{n_q} (1 + 2v_2^q \cos 2\phi_q) \approx 1 + 2n_q v_2^q \cos 2\Delta\phi \cos 2\phi_h. \quad (6)$$

Thus the hadron v_2 is given by

$$v_2^h(p_\perp^h) = n_q v_2^q(p_\perp^q) \cos 2\Delta\phi. \quad (7)$$

One may verify that this relationship, with the kinematics in Fig. 3, can approximately describe the v_2 relationship between pion (and proton) at $p_\perp = 1$ GeV/ c and the constituent quarks in Fig. 4. One can also verify Eq. (7) with the ρ v_2 shown later in Fig. 6. Note that we have simplified the above algebraic derivation by replacing the probability integrals with the average p_\perp ’s and ϕ ’s.

Clear mass splitting is observed for hadrons right after hadronization. Although v_2 is largely from the escape mechanism, there does exist a contribution from hydrodynamics in AMPT [30, 31]. Thus we also carry out the test calculations with no collective anisotropic flow by randomizing the outgoing parton azimuthal directions after each parton-parton scattering as in Ref. [30, 31]. The results are shown in Fig. 4 right panel. In the ϕ -randomized case, the parton azimuthal angles are randomized and hence their v_2 is zero; thus the final-state

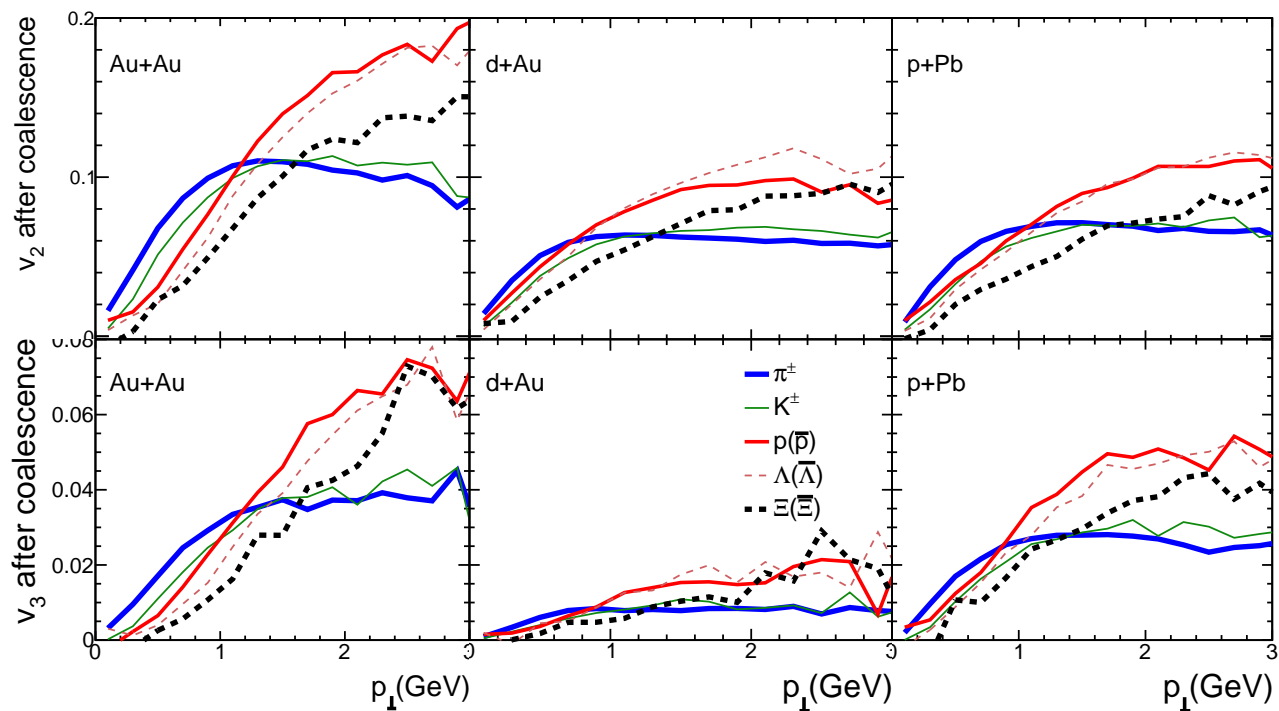


FIG. 2: (Color online) *Mass splitting from coalescence*. Primordial hadron v_n as a function of p_{\perp} right after coalescence hadronization before hadronic rescatterings take place in AMPT with string melting. Three systems are shown: $b = 6.6\text{-}8.1$ fm Au+Au collisions at $\sqrt{s_{\text{NN}}} = 200$ GeV (left column), $b = 0$ fm d+Au collisions at 200 GeV (middle column), and $b = 0$ fm p+Pb at 5 TeV (right column); v_2 results are shown in upper panels and v_3 in lower panels. Thick solid curves are for charged pions, thin solid curves for charged kaons, medium thick solid curves for (anti-)protons, thin dashed curves for $\Lambda(\bar{\Lambda})$, and thick dashed curves for $\Xi(\bar{\Xi})$.

freezeout anisotropy is entirely due to the anisotropic escape mechanism. Mass splitting is also observed. Thus, the mass splitting is not a unique signature of collective anisotropic flow or hydrodynamics. It is mainly due to kinematics in the coalescence process in the transport model.

V. EFFECTS OF DECAYS

After hadronization, particles interact both inelastically and elastically, and unstable particles gradually decay. Measured in detector are particles after interactions cease and after decays. The final freezeout particles in AMPT include all strong decays of resonances but no electromagnetic or weak decays by default (except for the Σ^0 decay in order to include its feed down to Λ) [26]. Shown in Fig. 4 are v_2 of primordial hadrons (obtained right after the quark coalescence in the AMPT evolution), not freezeout hadrons after resonance decays. To see the effect of decays on v_2 , we set the maximum hadronic stage to $t_{\text{max}} = 0.6$ fm in AMPT (parameter NTMAX=3) so the hadronic rescatterings are turned off. We then obtain the final-state hadron v_2 after decays

which are handled automatically by AMPT.

Figure 5 shows the fraction of primordial pions and primordial protons as a function of p_{\perp} . Figure 6 left panel shows the v_2 of primordial pions, that of ρ 's, that of the ρ -decay pions, and that of the all pions. The middle panel shows the corresponding results for kaons where the K^* decay channel is studied. The right panel shows those of protons where the decay channel is $\Delta \rightarrow p\pi$. At low p_{\perp} heavier particles have smaller v_2 after the coalescence hadronization (c.f. Fig.2). The decay product v_2 is usually smaller than their parent v_2 as shown in Fig. 6. As a result, the v_2 's of final-state hadrons including decay products are smaller than (or closely follow) those of the primordial particles. This reduction effect is stronger in pions than protons, because more fraction of pions come from resonance decays than protons and because the protons retain more of the parent v_2 than pions due to kinematics. Figure 7 shows the hadron v_2 and v_3 including contributions from decay products as a function of p_{\perp} . The reduction in v_n is evident in Fig. 7 as opposed to Fig 2 where only the primordial hadron v_n 's are shown. Before of the larger reduction in pion v_n than in proton v_n due to decays, the amount of mass-splitting is reduced. Depending on the magnitude

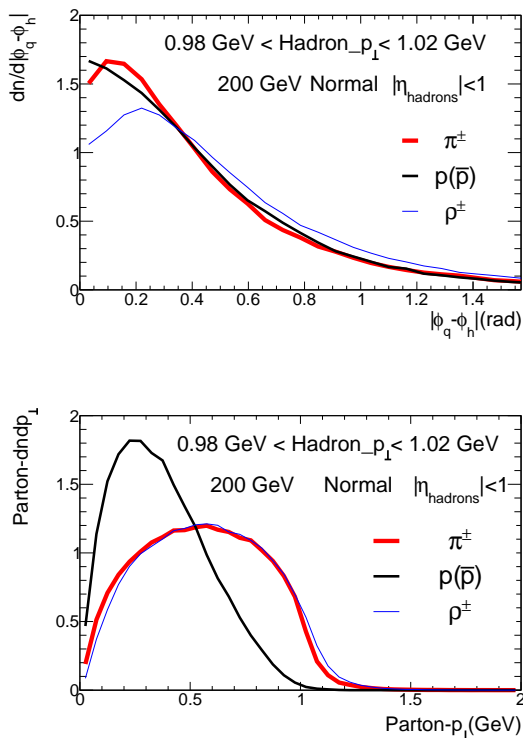


FIG. 3: (Color online) *Coalescence kinematics*. Final-state p_{\perp} (upper panel) and azimuthal opening angle (lower panel) distributions of constituent (anti)quarks forming π , ρ , and (anti)-proton. The constituent quark opening angle is defined to be the absolute value of the quark azimuthal angle (ϕ_q) relative to the hadron's (ϕ_h). Shown are AMPT (with string melting) results of $b = 6.6-8.1$ fm Au+Au collisions at 200 GeV.

of this reduction, the mass splitting between primordial hadrons (right after coalescence) may or may not survive once including the decay products. So in general the mass splitting effect decreases after including decay products, as shown in Fig. 7 compared to Fig. 2.

VI. MASS SPLITTING FROM HADRONIC RESCATTERINGS

Another source of mass splitting of v_n comes from hadronic rescatterings. In the following we study v_n as a function of the degree of hadronic rescatterings. We achieve this by varying the maximum allowed time, t_{\max} , of the hadronic interaction stage in AMPT. At t_{\max} , the hadronic evolution in AMPT is forced to end. So t_{\max} can be considered as a qualitative indicator of the amount of hadronic rescatterings. Note that there is no cut-off time for the partonic evolution in AMPT.

Figure 8 upper panels show freezeout pion, kaon, proton v_2 , as well as that of all charged hadrons, in mid-

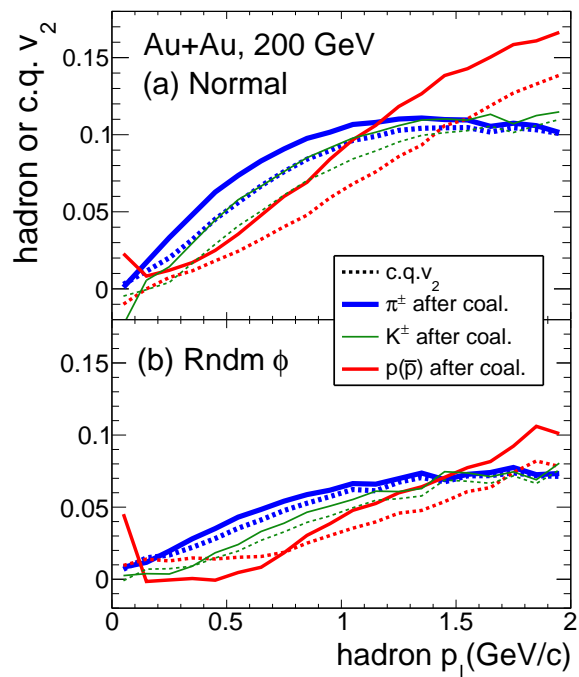


FIG. 4: (Color online) *Conversion of constituent quark v_2 into hadron v_2 by coalescence*. Primordial hadron and constituent quark v_2 , both plotted as a function of the hadron p_{\perp} . The hadron v_2 is taken before any hadronic rescattering and the constituent quark v_2 is taken just before coalescence. Shown are both normal (upper panel) and ϕ -randomized (lower panel) AMPT (with string melting) results for $b = 6.6-8.1$ fm Au+Au collisions at 200 GeV.

central Au+Au collisions versus p_{\perp} for various t_{\max} values. The pion v_2 increases with the amount of rescattering while proton v_2 decreases; the kaon v_2 does not change significantly. This may be understood as follows. Because of interactions between pions and protons, they tend to flow together at the same velocity. Thus, the same-velocity pions and protons (i.e. small p_{\perp} pions and large p_{\perp} protons) will tend to have the same anisotropy. This will yield lower v_2 for protons and higher v_2 for pions at the same p_{\perp} value. This should happen even when there is no net gain in v_2 for the charged hadrons. Whether there is an overall gain in v_2 of the charged hadrons depends on the configuration geometry. Figure 8 shows indeed a small increase in the overall charged hadron v_2 , and this is due to the remaining finite configuration space eccentricity before hadronic scatterings take place, as we shall discuss below.

Figure 8 also shows, in the lower panels, the results from d +Au collisions. There, pion v_2 increases significantly with hadronic scattering, the proton v_2 remains roughly unchanged, while the kaon v_2 change is in-between. This is a net effect of the splitting due to pion-proton interactions (i.e. increase in pion v_2 and de-

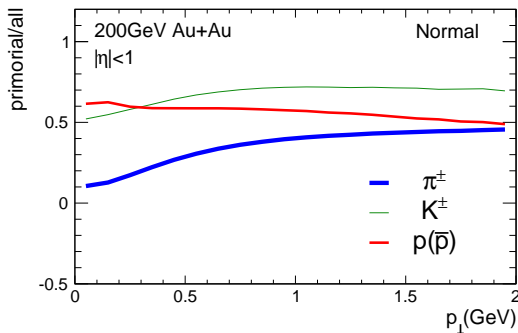


FIG. 5: (Color online) *Decay contributions*. Fraction of primordial hadrons in $b = 6.6\text{-}8.1$ fm Au+Au collisions at 200 GeV in AMPT (with string melting). Hadronic rescattering is turned off.

crease in proton v_2) and an overall gain of v_2 for charged hadrons. The overall gain in the charged hadron v_2 is larger in d +Au than Au+Au collisions, and this is due to the larger eccentricity in the d +Au system.

As can be seen in Fig. 8, v_2 continues to develop after hadronization in Au+Au as well as d +Au collisions. In Au+Au collisions the development happens mainly during 5-10 fm/c after hadronization, while in d +Au collisions the development happens earlier (mainly before 5 fm/c). The spatial anisotropy is self-quenched due to development of momentum space anisotropy. The further increase of overall charged hadron v_2 in Fig. 8 suggests that the spatial anisotropy is not completely quenched at the time right after hadronization; a finite spatial anisotropy is present at the beginning of hadronic scatterings which result in the further development of v_n .

We elaborate this further by examining the increase in v_2 as a function of the remaining eccentricity after hadronization (ϵ_2^{had}), i.e. the starting eccentricity for hadronic rescattering. This is shown in Fig. 9 for both Au+Au and d +Au collisions. Since a typical AMPT evolution around mid-rapidity essentially ends before the time of 30 fm/c, we evaluate the increase in v_2 from hadronic scatterings as $\Delta v_2 = v_2^{30\text{fm}/c} - v_2^{0.6\text{fm}/c}$. The ϵ_2^{had} value is calculated with respect to the initial configuration space Ψ_2 , as is v_2 . We have verified that the hadron v_2 right after the coalescence hadronization (and for that matter, also the v_2 at final freezeout) is proportional to the initial eccentricity (ϵ_2)—which is also calculated with respect to the initial Ψ_2 —except when ϵ_2 is large (close to one). The ϵ_2^{had} value is positively correlated with the ϵ_2 value in Au+Au collisions, while the correlation is weak in d +Au collisions.

Figure 9 show that, in the ϵ_2^{had} range of 0-0.2 in Au+Au and 0-0.5 in d +Au, Δv_2 appears to linearly increase with ϵ_2^{had} . At large positive ϵ_2^{had} the statistics are poor and ϵ_2^{had} may not reflect a bulk geometry any more. At negative ϵ_2^{had} events are also rare. On average, $\langle \epsilon_2^{\text{had}} \rangle$ is 0.11

in Au+Au and 0.42 in d +Au collisions, starting from an initial $\langle \epsilon_2 \rangle$ of 0.29 and 0.53, respectively. The geometry anisotropy is thus not quenched completely after partonic interactions in Au+Au collisions; the reduction in eccentricity in d +Au collisions is even smaller, indicating a shorter partonic stage. The remaining spatial anisotropy is smaller in Au+Au than in d +Au, and this results in a smaller v_2 gain during the hadronic rescattering stage in Au+Au than in d +Au, as observed in Fig. 8.

It is interesting to note that Δv_2 is finite for $\epsilon_2^{\text{had}} = 0$ events, where one would naively expect $\Delta v_2 = 0$ (i.e. no further increase in v_2). This would indeed be true if the initial hadron $v_2^{0.6\text{fm}/c}$ (before hadronic scatterings) was zero, analogous to the initial parton $v_n^{\text{ini}} \equiv 0$ in AMPT (before partonic scatterings). For finite initial $v_2^{0.6\text{fm}/c} > 0$, which is the case here, it is unnecessarily true that v_2 would not further develop.

Figure 10 shows hadron v_2 as a function of p_\perp before hadronic scatterings but including resonance decays in dashed curves and v_2 of freezeout hadrons after hadronic scatterings in solid curves. This figure illustrates the effect of hadronic scatterings on the mass splitting of v_2 . As shown, hadronic scatterings make significant contributions to the mass splitting in the final-state hadron v_2 . Meanwhile the absolute gain of the v_2 magnitude is relatively small during the hadronic stage.

VII. SUMMARY ON THE ORIGINS OF MASS SPLITTING

Figure 11 shows final-state hadron v_2 and v_3 at freezeout as a function of p_\perp in Au+Au and d +Au collisions at 200 GeV and p +Pb collisions at 5 TeV. The mass splitting of v_n at low p_\perp is obvious in Au+Au collisions; although not as obvious in small systems, there is generally mass splitting in v_n at low p_\perp . There is also split in v_n at high p_\perp , likely more due to baryon-meson rather than the mass difference, which is outside the scope of this paper. Several sources contribute to the mass splitting in AMPT as we showed in the previous sections.

To summarize the origins of the mass splitting of v_2 , we plot in Fig. 12 the v_2 of pions, kaons, and (anti-)protons as well as charged hadrons (sum of charged pions, kaons, protons and antiprotons), within a fixed p_\perp bin of $0.8 < p_\perp < 1.2$ GeV/c, as an example. Different stages of the collision system evolution are shown: (i) right after the quark coalescence hadronization including only primordial particles (data points plotted to the left of $t = 0$); (ii) right after coalescence hadronization but including decay products (data points plotted at $t = 0.6$ fm/c); (iii) after various degrees of hadronic scatterings, which are obtained from freezeout particles by setting t_{max} to the corresponding time value plotted. As shown in Fig. 12, most of the final measured v_2 is built up in the partonic phase; additional gain in v_2 from hadronic scatterings is small. On the other hand, although there is a significant mass splitting in primordial

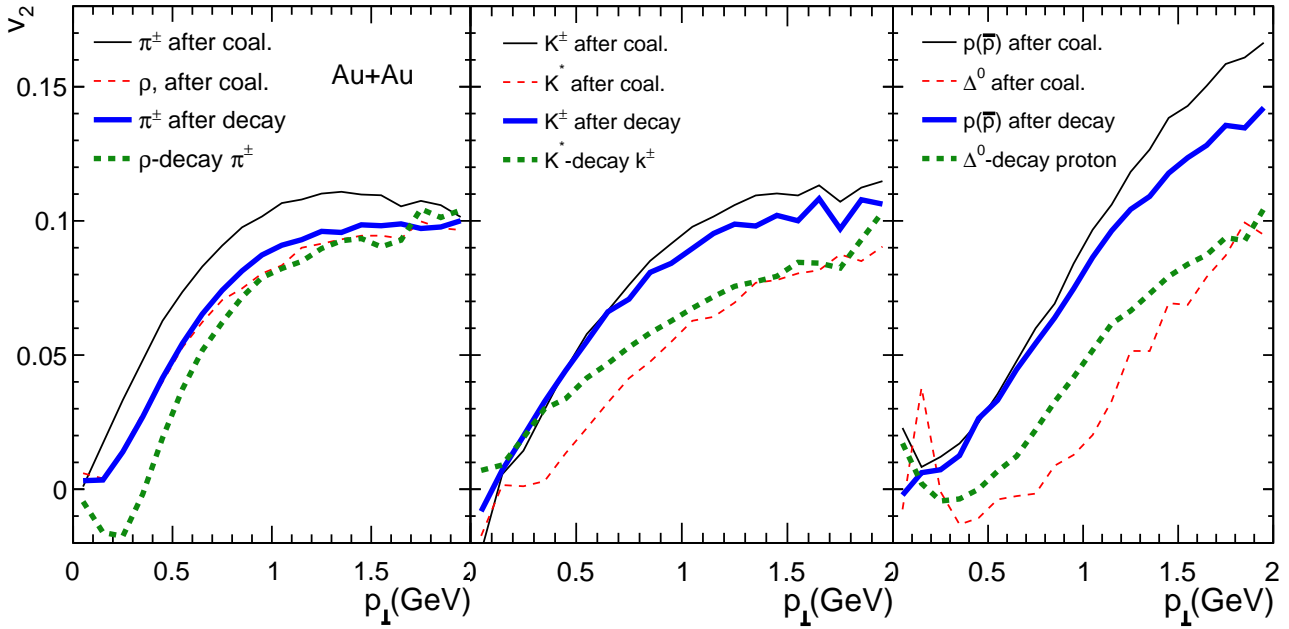


FIG. 6: (Color online) *Effect of decays on v_2* . The v_2 of primordial hadrons (thin solid curves), resonances (thin dashed curves), and decay products (thick dashed curves), and the net v_2 including both the primordial hadrons and decay products (thick solid curves). Shown are $b = 6.6$ - 8.1 fm Au+Au collisions at 200 GeV by AMPT (with string melting). Hadronic scattering is turned off. The left panel shows results for π and ρ , the middle panel for K and K^* , and the right panel for $p(\bar{p})$ and $\Delta(\bar{\Delta})$.

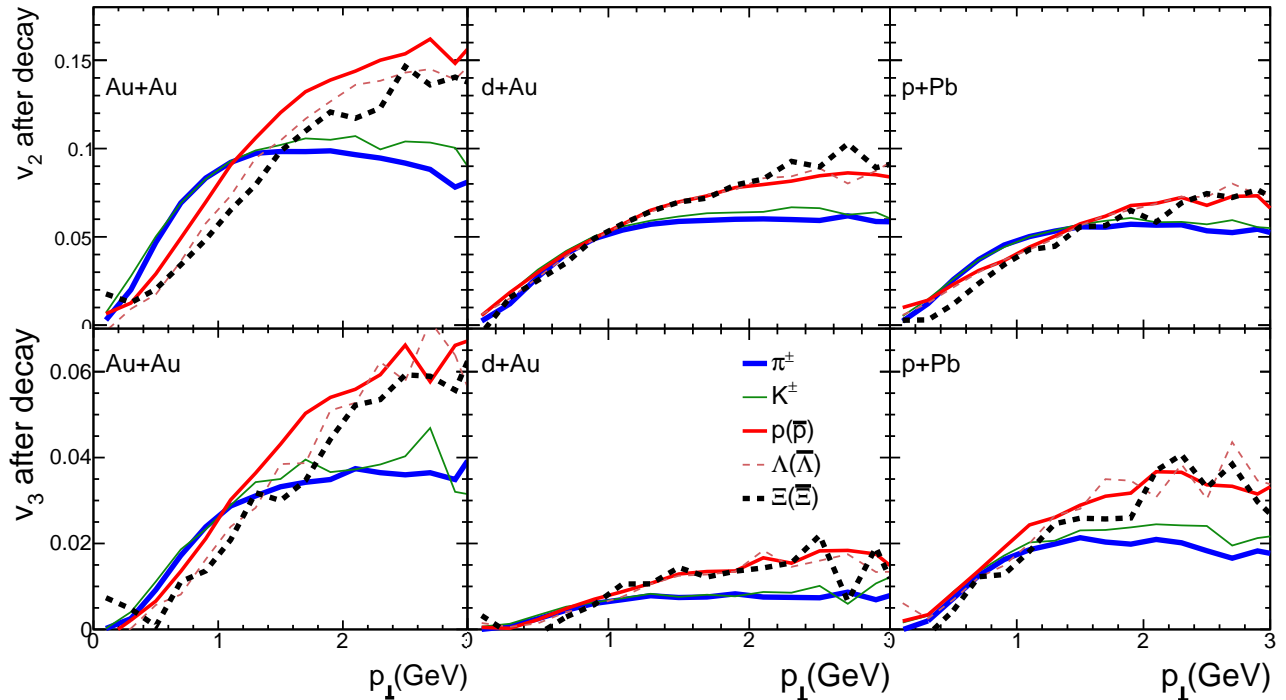


FIG. 7: (Color online) *Effect of decays on mass splitting*. Hadron v_n including both primordial hadrons and decay products. Three systems are shown: $b = 6.6$ - 8.1 fm Au+Au collisions at $\sqrt{s_{NN}} = 200$ GeV (left column), $b = 0$ fm d+Au collisions at 200 GeV (middle column), and $b = 0$ fm p+Pb at 5 TeV (right column); v_2 results are shown in upper panels and v_3 in lower panels. Results are from AMPT (with string melting) with hadronic rescatterings turned off. Thick solid curves are for charged pions, thin solid curves for charged kaons, medium thick solid curves for (anti-)protons, thin dashed curves for $\Lambda(\bar{\Lambda})$, and thick dashed curves for $\Xi(\bar{\Xi})$.

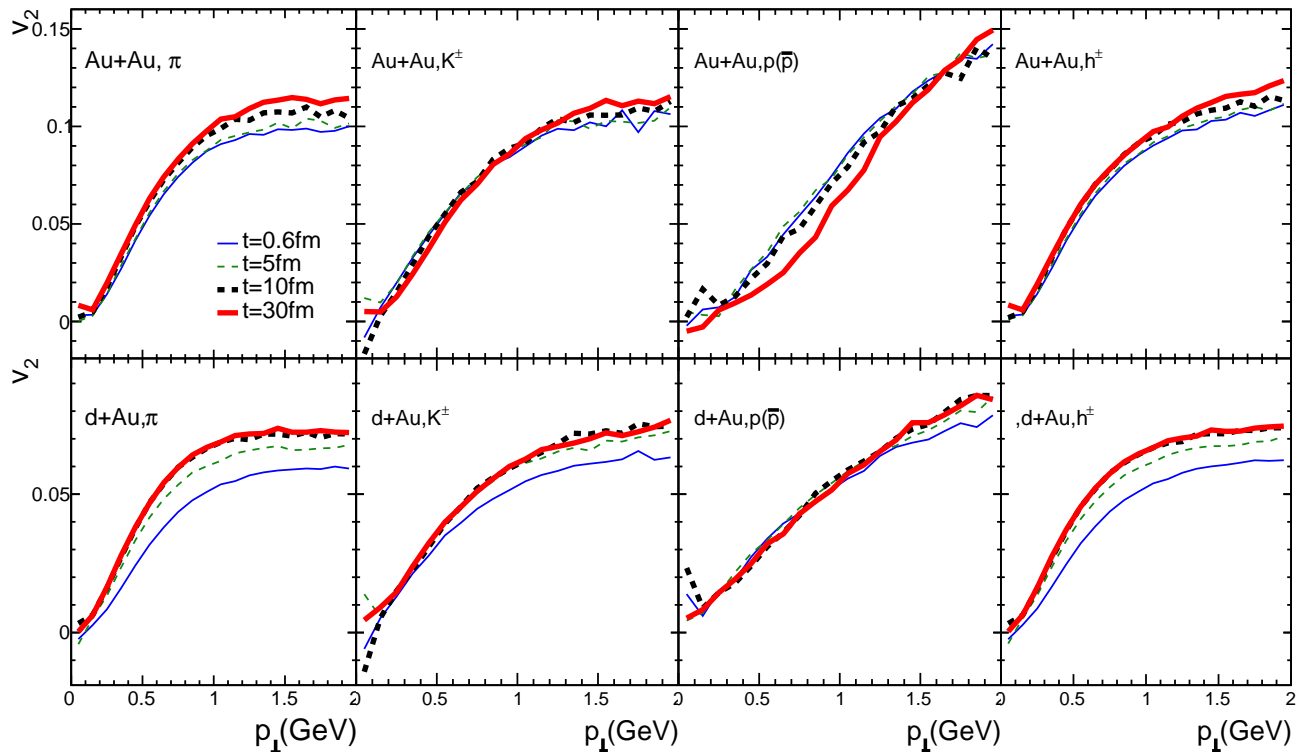


FIG. 8: (Color online) *Effects of hadronic rescatterings on v_2* . Hadron v_2 as a function of p_\perp at different stages of hadronic rescattering in AMPT (with string melting). The v_2 are from final-state hadrons including resonance decays, where the final freeze-out is controlled by the maximum allowed time (t_{\max}) for the hadronic stage. Shown are for charged pions (first column), charged kaons (second column), (anti-)protons (third column), and unidentified charged hadrons (last column) in $b = 6.6\text{-}8.1$ fm Au+Au collisions at 200 GeV (upper panels) and $b = 0$ fm d +Au collisions at 200 GeV (lower panels).

hadron v_2 right after hadronization due to kinematics in the coalescence procedure, the mass splitting is reduced if decay products are included in v_2 . In other words, the mass splitting before hadronic rescatterings is relatively small. This small mass splitting does not change significantly during the first 5 fm/c since the partonic stage dominates the early evolution. A significant mass splitting is built up during the 5-10 fm/c of hadronic rescattering. After 10 fm/c there is no further change in v_2 in d +Au collisions; in Au+Au there is still a modest increase in the size of mass splitting.

Note that previous hadron cascade studies [39–41], including a recent one with free-streaming evolution coupled to a hadron cascade [16], have shown that the v_2 mass splitting can be generated by hadronic rescatterings. However, typically the overall v_2 magnitudes from hadronic scatterings significantly underestimate the measured v_2 [16, 40, 41], while the study that roughly reproduces the v_2 magnitudes at low p_\perp has used hadron degrees of freedom at very high energy densities [39]. On the other hand, the overall v_2 in this multi-phase model study is mostly generated by partonic rescatterings at high energy densities [30], while the v_2 mass splitting

mostly comes from the later hadronic scatterings. In addition, our model has already been shown to reasonably reproduce particle yields, p_\perp spectra, and v_2 of low- p_\perp pions and kaons in Au+Au collisions [28].

VIII. CONCLUSIONS

Previous studies have shown that the measured azimuthal anisotropies v_n in heavy ion as well as small system collisions at low p_\perp can be well described by both hydrodynamics and a multi-phase transport model AMPT. The mass splitting of v_n is considered as a strong evidence for hydrodynamic collective flow. However, a recent study [30] indicates that the anisotropic escape mechanism is the major source of v_n in transport models including AMPT, and in particular, the only source of v_n in the ϕ -randomized test of AMPT.

We have studied the development of the v_2 mass splitting at different stages of nuclear collisions in AMPT. The main results of our study have been published in Ref. [32]. The present work provides extensive details to the published study using heavy ion collisions at RHIC,

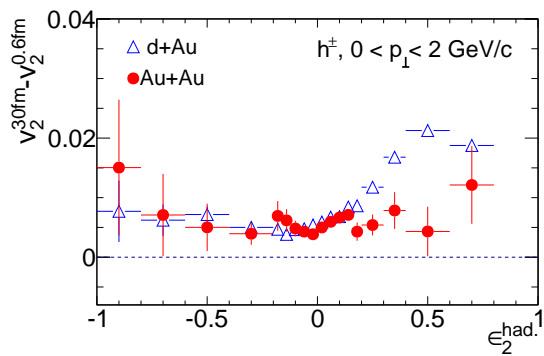


FIG. 9: (Color online) *Connection to hadronic eccentricity.* Gain in charged hadron v_2 due to hadronic rescatterings from hadronization ($t_{\max} = 0.6$ fm/c) to final freezeout ($t_{\max} = 30$ fm/c) as a function of the configuration space eccentricity of hadrons right after hadronization (ϵ_2^{had}) in $b = 6.6\text{--}8.1$ fm Au+Au (upper panel) and $b = 0$ fm d+Au (lower panel) collisions at 200 GeV. Both ϵ_2^{had} and v_2 are calculated with respect to the initial parton Ψ_2 . The ϵ_2^{had} measures the eccentricity of hadrons at initial state before hadronic rescatterings (i.e. right after hadronization). The v_2 are from final-state hadrons including resonance decays, where the final freeze-out is controlled by the maximum allowed time (t_{\max}) for the hadronic stage.

as well as extends the study to p +Pb collisions at the LHC. We conclude that the mass splitting of v_n is partly due to coalescence hadronization but more importantly due to hadronic rescatterings [32]. We find that, while the v_2 amplitude is dominantly developed during the partonic cascading stage, the mass splitting is relatively small right after hadronization, especially after including resonance decays. This mass splitting is produced by kinematics in the coalescence process. We then demonstrate that the majority of the mass splitting is developed in the hadronic rescattering stage, even though the gain in the overall v_2 amplitude of charged particles is small. These qualitative conclusions are the same as those from hybrid models that couple hydrodynamics to a hadron cascade. In addition, we found no qualitative difference between Au+Au collisions and d+Au collisions. We conclude that the mass splitting of v_2 cannot be considered as a unique signature of hydrodynamic collective flow, and the v_2 mass splitting cannot distinguish whether the elliptic flow is generated mainly from hydrodynamics or the anisotropic parton escape.

Acknowledgments

This work is supported in part by US Department of Energy Grant No. DE-FG02-88ER40412 (LH,FW,WX) and No. DE-FG02-13ER16413 (DM). HL acknowledges financial support from the China Scholarship Council.

-
- [1] I. Arsene et al. Quark gluon plasma and color glass condensate at RHIC? The Perspective from the BRAHMS experiment. *Nucl.Phys.*, A757:1–27, 2005.
 - [2] B.B. Back et al. The PHOBOS perspective on discoveries at RHIC. *Nucl.Phys.*, A757:28–101, 2005.
 - [3] John Adams et al. Experimental and theoretical challenges in the search for the quark gluon plasma: The STAR Collaboration’s critical assessment of the evidence from RHIC collisions. *Nucl.Phys.*, A757:102–183, 2005.
 - [4] K. Adcox et al. Formation of dense partonic matter in relativistic nucleus-nucleus collisions at RHIC: Experimental evaluation by the PHENIX collaboration. *Nucl.Phys.*, A757:184–283, 2005.
 - [5] Berndt Muller, Jurgen Schukraft, and Boleslaw Wyslouch. First Results from Pb+Pb collisions at the LHC. *Ann.Rev.Nucl.Part.Sci.*, 62:361–386, 2012.
 - [6] Ulrich Heinz and Raimond Snellings. Collective flow and viscosity in relativistic heavy-ion collisions. *Ann.Rev.Nucl.Part.Sci.*, 63:123–151, 2013.
 - [7] Charles Gale, Sangyong Jeon, and Bjoern Schenke. Hydrodynamic Modeling of Heavy-Ion Collisions. *Int.J.Mod.Phys.*, A28:1340011, 2013.
 - [8] B.I. Abelev et al. Systematic Measurements of Identified Particle Spectra in pp , d +Au and Au+Au Collisions from STAR. *Phys.Rev.*, C79:034909, 2009.
 - [9] Jean-Yves Ollitrault. Anisotropy as a signature of transverse collective flow. *Phys.Rev.*, D46:229–245, 1992.
 - [10] Miklos Gyulassy and Larry McLerran. New forms of QCD matter discovered at RHIC. *Nucl.Phys.*, A750:30–63, 2005.
 - [11] R. Andrade, F. Grassi, Yojiro Hama, T. Kodama, and Jr. Socolowski, O. On the necessity to include event-by-event fluctuations in experimental evaluation of elliptical flow. *Phys.Rev.Lett.*, 97:202302, 2006.
 - [12] B. Alver and G. Roland. Collision geometry fluctuations and triangular flow in heavy-ion collisions. *Phys.Rev.*, C81:054905, 2010. Erratum-ibid. **C82**, 039903 (2010).
 - [13] Fred Cooper and Graham Frye. Comment on the Single Particle Distribution in the Hydrodynamic and Statistical Thermodynamic Models of Multiparticle Production. *Phys.Rev.*, D10:186, 1974.
 - [14] Tetsufumi Hirano, Ulrich W. Heinz, Dmitri Kharzeev, Roy Lacey, and Yasushi Nara. Mass ordering of differential elliptic flow and its violation for phi mesons. *Phys.Rev.*, C77:044909, 2008.
 - [15] Huichao Song, Steffen A. Bass, and Ulrich Heinz. Viscous QCD matter in a hybrid hydrodynamic+Boltzmann approach. *Phys.Rev.*, C83:024912, 2011.
 - [16] Paul Romatschke. Collective flow without hydrodynamics: simulation results for relativistic ion collisions. *Eur.Phys.J.*, C75(9):429, 2015.
 - [17] Vardan Khachatryan et al. Observation of Long-Range Near-Side Angular Correlations in Proton-Proton Collisions at the LHC. *JHEP*, 1009:091, 2010.

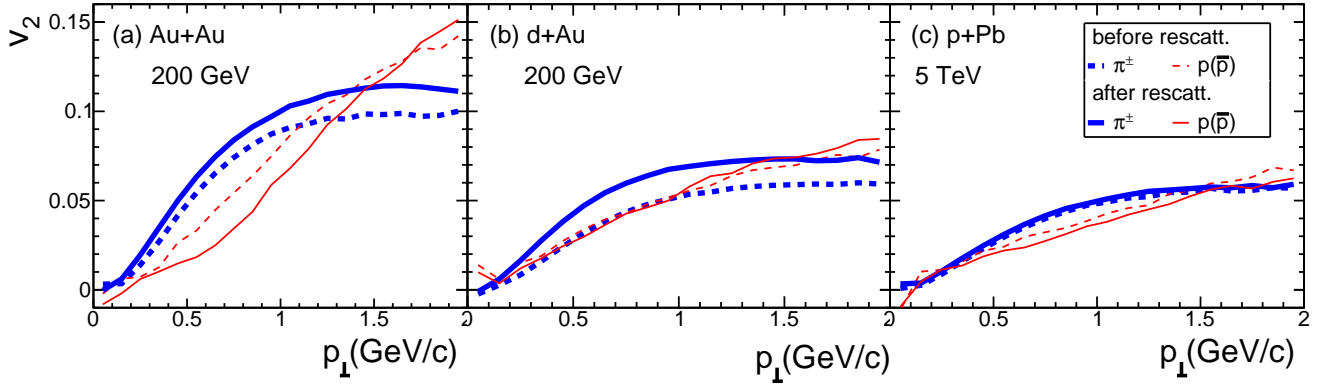


FIG. 10: (Color online) *Effect of hadronic rescatterings on mass splitting.* Charged pions (thick curves) and (anti-)proton (thin curves) v_2 as a function of p_{\perp} before (dashed curves) and after (solid curves) hadron rescatterings in AMPT (with string melting). The effects of resonance decays are included. Three systems are shown: $b = 6.6\text{--}8.1$ fm Au+Au collisions at $\sqrt{s_{NN}} = 200$ GeV (left column), $b = 0$ fm d+Au collisions at 200 GeV (middle column), and $b = 0$ fm p+Pb at 5 TeV (right column).

- [18] Serguei Chatrchyan et al. Observation of long-range near-side angular correlations in proton-lead collisions at the LHC. *Phys.Lett.*, B718:795–814, 2013.
- [19] Betty Abelev et al. Long-range angular correlations on the near and away side in p-Pb collisions at $\sqrt{s_{NN}}=5.02$ TeV. *Phys.Lett.*, B719:29–41, 2013.
- [20] Georges Aad et al. Observation of Associated Near-side and Away-side Long-range Correlations in $\sqrt{s_{NN}}=5.02$ TeV Proton-lead Collisions with the ATLAS Detector. *Phys.Rev.Lett.*, 110:182302, 2013.
- [21] A. Adare et al. Measurement of long-range angular correlation and quadrupole anisotropy of pions and (anti)protons in central d+Au collisions at $\sqrt{s_{NN}}=200$ GeV. *Phys.Rev.Lett.*, 114:192301, 2015.
- [22] L. Adamczyk et al. Long-range pseudorapidity dihadron correlations in d+Au collisions at $\sqrt{s_{NN}} = 200$ GeV. *Phys.Lett.*, B747:265–271, 2015.
- [23] Piotr Bozek. Elliptic flow in proton-proton collisions at $\sqrt{S} = 7$ TeV. *Eur.Phys.J.*, C71:1530, 2011.
- [24] Piotr Bozek and Wojciech Broniowski. Correlations from hydrodynamic flow in p-Pb collisions. *Phys.Lett.*, B718:1557–1561, 2013.
- [25] Bin Zhang, C.M. Ko, Bao-An Li, and Zi-wei Lin. A multiphase transport model for nuclear collisions at RHIC. *Phys.Rev.*, C61:067901, 2000.
- [26] Zi-Wei Lin, Che Ming Ko, Bao-An Li, Bin Zhang, and Subrata Pal. A Multi-phase transport model for relativistic heavy ion collisions. *Phys.Rev.*, C72:064901, 2005.
- [27] Zi-wei Lin and C.M. Ko. Partonic effects on the elliptic flow at RHIC. *Phys.Rev.*, C65:034904, 2002.
- [28] Zi-Wei Lin. Evolution of transverse flow and effective temperatures in the parton phase from a multi-phase transport model. *Phys.Rev.*, C90:014904, 2014.
- [29] Adam Bzdak and Guo-Liang Ma. Elliptic and triangular flow in p+Pb and peripheral Pb+Pb collisions from parton scatterings. *Phys.Rev.Lett.*, 113:252301, 2014.
- [30] Liang He, Terrence Edmonds, Zi-Wei Lin, Feng Liu, Denes Molnar, and Fuqiang Wang. Anisotropic parton escape is the dominant source of azimuthal anisotropy in transport models. *Phys. Lett.*, B753:506–510, 2016.
- [31] Zi-Wei Lin, Liang He, Terrence Edmonds, Feng Liu, Denes Molnar, and Fuqiang Wang. Elliptic Anisotropy v_2 May Be Dominated by Particle Escape instead of Hydrodynamic Flow. 2015.
- [32] Hanlin Li, Liang He, Zi-Wei Lin, Denes Molnar, Fuqiang Wang, and Wei Xie. Origin of the mass splitting of elliptic anisotropy in A Multi-Phase Transport model. arXiv:1502.05572, Phys. Rev. C (R) in press. 2016.
- [33] Bin Zhang. ZPC 1.0.1: A Parton cascade for ultrarelativistic heavy ion collisions. *Comput.Phys.Commun.*, 109:193–206, 1998.
- [34] Yongseok Oh, Zi-Wei Lin, and Che Ming Ko. Deuteron production and elliptic flow in relativistic heavy ion collisions. *Phys. Rev.*, C80:064902, 2009.
- [35] Jean-Yves Ollitrault. Determination of the reaction plane in ultrarelativistic nuclear collisions. *Phys.Rev.*, D48:1132–1139, 1993.
- [36] S. Voloshin and Y. Zhang. Flow study in relativistic nuclear collisions by Fourier expansion of Azimuthal particle distributions. *Z.Phys.*, C70:665–672, 1996.
- [37] Kai Xiao, Feng Liu, and Fuqiang Wang. Event-plane decorrelation over pseudo-rapidity and its effect on azimuthal anisotropy measurement in relativistic heavy-ion collisions. *Phys.Rev.*, C87:011901, 2013.
- [38] Zi-Wei Lin. Quark Coalescence with Quark Number Conservation and the Effect on Quark-Hadron Scaling. *J. Phys.*, G38:075002, 2011.
- [39] G. Burau, J. Bleibel, C. Fuchs, Amand Faessler, L. V. Bravina, and E. E. Zabrodin. Anisotropic flow of charged and identified hadrons in the quark-gluon string model for Au + Au collisions at $s(NN)^{(1/2)} = 200\text{-GeV}$. *Phys. Rev.*, C71:054905, 2005.
- [40] Hannah Petersen, Qingfeng Li, Xianglei Zhu, and Marcus Bleicher. Directed and elliptic flow in heavy ion collisions at GSI-FAIR and CERN-SPS. *Phys. Rev.*, C74:064908, 2006.
- [41] You Zhou, Xiangrong Zhu, Pengfei Li, and Huichao Song. Investigation of possible hadronic flow in $\sqrt{s_{NN}} = 5.02$

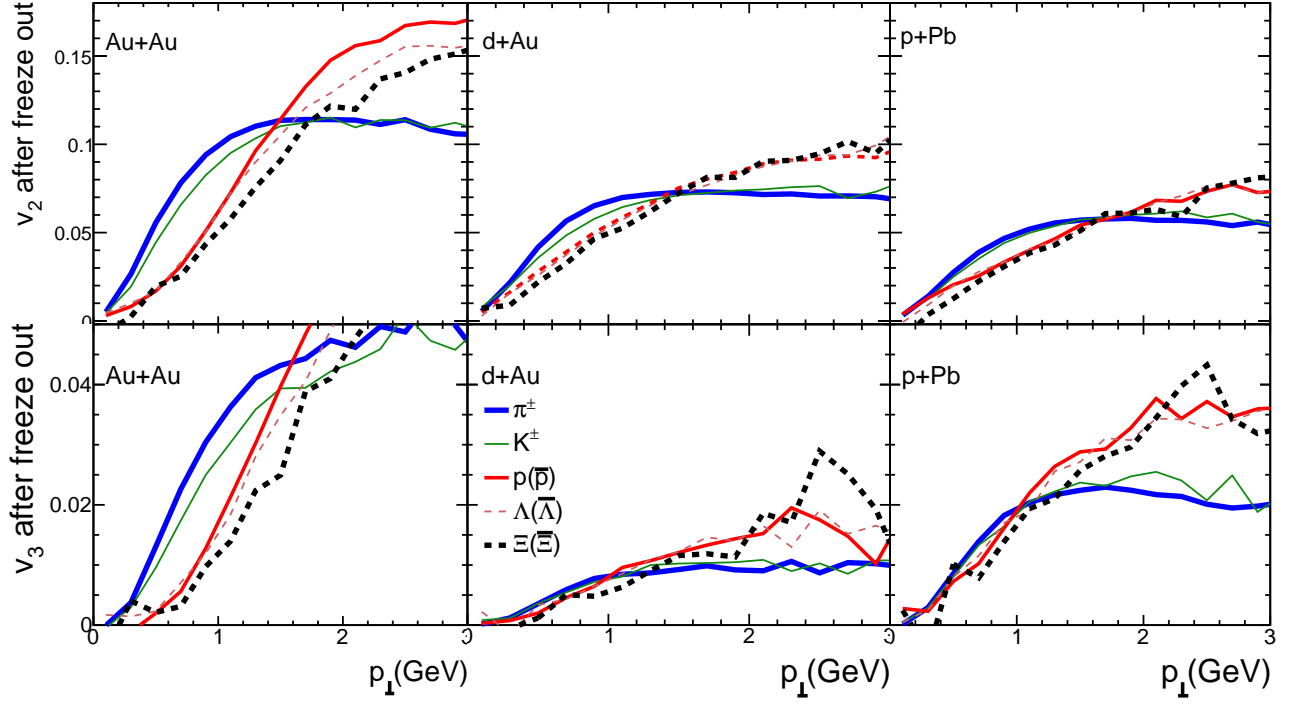


FIG. 11: (Color online) *Mass splitting at freezeout*. Final-state freezeout hadron v_n as a function of p_{\perp} from AMPT (with string melting). Decay products are included. Three systems are shown: $b = 6.6\text{--}8.1$ fm Au+Au collisions at $\sqrt{s_{NN}} = 200$ GeV (left column), $b = 0$ fm d+Au collisions at 200 GeV (middle column), and $b = 0$ fm p+Pb at 5 TeV (right column); v_2 results are shown in upper panels and v_3 in lower panels. Thick solid curves are for charged pions, thin solid curves for charged kaons, medium thick solid curves for (anti-)protons, thin dashed curves for $\Lambda(\bar{\Lambda})$, and thick dashed curves for $\Xi(\bar{\Xi})$.

TeV $p - Pb$ collisions. *Phys. Rev.*, C91:064908, 2015.

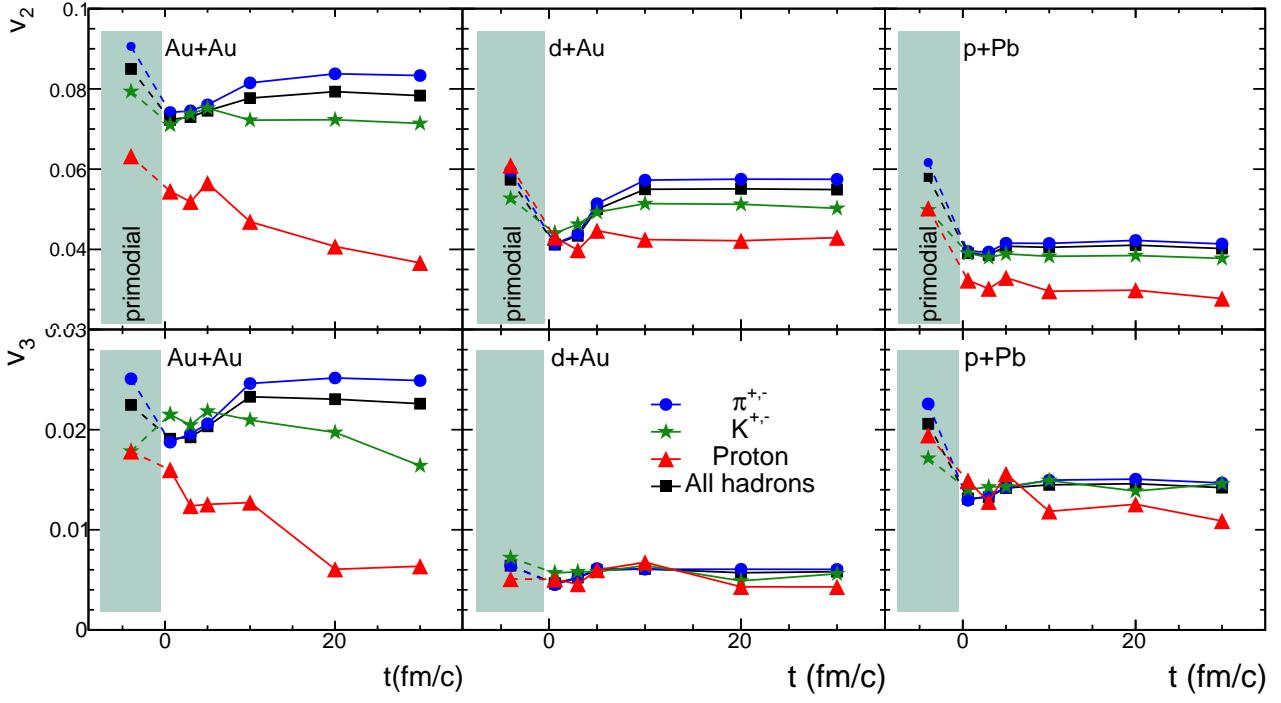


FIG. 12: (Color online) *Origins of v_n mass splitting*. The v_n of charged pions, charged kaons, (anti-)protons, and unidentified charged hadrons within a fixed $0.8 < p_\perp < 1.2$ GeV/c bin, as an example, at different stages of the collision evolution: those plotted within the shaded areas denoting results right after coalescence hadronization including only primordial particles, $t_{\max} = 0.6$ fm/c denoting results right after hadronization but including decay products, and the various t_{\max} values for hadronic rescattering times. The majority of v_n is built up in the partonic stage, with modest mass splitting, especially after including resonance decays. Hadronic rescatterings have only minor contributions to the overall v_n magnitude, but generate the majority of the mass splitting of v_n .